

RESEARCH

Open Access



In silico investigation of HCV and RNA synthesis inhibitor antibiotic drugs as potential inhibitors of SARS-CoV-2 main protease (Mpro)

Merusomayajula V. Kishore^{1*} , T. Siva Rao^{1*} and G. N. D. Kumari²

Abstract

Background Since December 2019, a global crisis has unfolded with the emergence of a new strain of coronavirus known as SARS-CoV-2. This pandemic has afflicted hundreds of millions of people worldwide, resulting in millions of fatalities. In response to this urgent healthcare crisis, extensive efforts have been made to discover inhibitors of the COVID-19 virus. Given the structural similarities between SARS-CoV-2 and HCV, drugs approved by the FDA for treating HCV were selected and subjected to in silico testing against the SARS-CoV-2 virus, with Remdesivir used as the standard for validation. Drug repurposing and phytochemical testing have also been conducted to identify potential candidates capable of inhibiting or suppressing the infection caused by the coronavirus. The time constraints imposed by the pandemic necessitated the in silico analysis of existing drug molecules against the coronavirus. Eleven HCV drugs approved by the FDA, along with one RNA synthesis inhibitor antibiotic drug, were tested using the in silico method due to their structural similarities with HCV and the SARS-CoV-2 virus.

Results Molecular docking and MD simulation studies were performed for all selected compounds. Binding energies, root-mean-square deviation, root-mean-square fluctuation, solvent-accessible surface area, radius of gyration, and molecular mechanics generalized born surface area were calculated. Based on docking and MD simulation studies all the selected compounds have shown good binding energy values with Mpro (PDB ID: 6LU7). No toxicity measurements are required for these drugs since they were previously tested prior to their approval by the FDA.

Conclusions This study shows that FDA-approved HCV drugs can be used as for SARS-COVID-19 inhibitors.

Keywords SARS-CoV-2 (Mpro), COVID-19, HCV drugs, Docking study, MD simulations

Background

In December 2019, the world faced a global crisis with the emergence of COVID-19, leading to widespread suffering. According to data from the worldometers database (<https://www.worldometers.info/coronavirus/>),

this pandemic resulted in 680,656,727 confirmed cases and 6,805,186 fatalities, impacting nearly every country worldwide. Common symptoms of COVID-19 include fever, fatigue, dry cough, shortness of breath and respiratory distress [1]. Studies have shown that COVID-19 patients with respiratory issues are at a higher risk of kidney impairment [2]. Given the associated risk factors and the lack of specific drugs developed to date for prevention, there is an urgent need for therapeutic strategies to address this disease [3]. Utilizing existing approved antiviral pharmaceuticals offers several advantages due to their well-studied pharmacokinetics, pharmacodynamics and safety profiles [4–7]. Drug repurposing has gained significance as it is anticipated to be a faster and

*Correspondence:

Merusomayajula V. Kishore
kishorechem6327@gmail.com

T. Siva Rao
sivaraotvalluri.16@gmail.com

¹ Department of Chemistry, AU College of Science and Technology, Andhra University, Visakhapatnam, Andhra Pradesh 530003, India

² Acharya Nagarjuna University, Guntur, India



© The Author(s) 2024. **Open Access** This article is licensed under a Creative Commons Attribution 4.0 International License, which permits use, sharing, adaptation, distribution and reproduction in any medium or format, as long as you give appropriate credit to the original author(s) and the source, provide a link to the Creative Commons licence, and indicate if changes were made. The images or other third party material in this article are included in the article's Creative Commons licence, unless indicated otherwise in a credit line to the material. If material is not included in the article's Creative Commons licence and your intended use is not permitted by statutory regulation or exceeds the permitted use, you will need to obtain permission directly from the copyright holder. To view a copy of this licence, visit <http://creativecommons.org/licenses/by/4.0/>.

more cost-effective approach. Initial research has suggested that a combination of lopinavir and ritonavir may have inhibitory effects on the virus, with numerous other antiviral medications also under investigation [8, 9]. Additionally, the potential therapeutic benefits of naturally occurring bioactive flavonoid molecules have been explored due to their diverse bioactivity and low toxicity [10, 11].

The SARS-CoV-2 virus, a positive-sense single-stranded RNA virus, encompasses a plethora of structural proteins such as accessory proteins and spike glycoprotein, in addition to several non-structural proteins encoded by its viral genome. Foremost among these non-structural proteins is the 3-chymotrypsin-like protease, accompanied by helicases, papain-like proteases and RNA-dependent RNA polymerase (RdRp) [12]. RdRp assumes a pivotal role in the replication process of SARS-CoV-2, making it a prime target for the development of antiviral medications, which have proven effective against various RNA viruses including Zika, Hepatitis C and other coronaviruses [13]. Notably, Remdesivir and Favipiravir have demonstrated efficacy in inhibiting SARS-CoV-2 replication by targeting RdRp and RNA polymerase in vitro [7, 8, 14]. Moreover, the viral replication process relies on the activity of the viral protease (Mpro), encoded by the retroviral RNA genome [15]. Targeting this enzyme with antiviral medications has shown promise in preventing viral replication by limiting the activity of Mpro and subsequently reducing the quantity of virus particles [15–17]. Among these medications, certain HIV-1 protease inhibitors like lopinavir and ritonavir have exhibited effectiveness in hindering SARS-CoV-2 from producing its major protease, presenting potential therapeutic avenues against COVID-19 [10].

Moreover, HCV belongs to the Flaviviridae family of viruses, whereas SARS-CoV-2 is classified within the Coronavirus family. Although SARS-CoV-2 and HCV are distinct viruses, they share the characteristic of being positive single-strand RNA viruses (+ssRNA) genetically. Remarkably, they exhibit similar immunological traits concerning host immune responses, which could offer insights into potential treatment strategies for COVID-19. Taken together, it is apparent that HCV, SARS-CoVs and possibly SARS-CoV-2s may share comparable pathophysiological aspects in terms of immune response [18]. Various approaches, including drug repurposing, sampling methods and genome comparison methods, are being explored to identify inhibitors for COVID-19 [32–35].

Recently, computer-aided drug design (CADD) has significantly expedited the process of drug discovery, leading to substantial reductions in costs, time and labor compared to traditional methods. Computational

drug screening, a component of CADD, efficiently sifts through compound libraries to identify potential drugs [19]. A structural-based drug design approach was employed to pinpoint promising drug candidates from selected ligands [31]. Leveraging the shared genetic characteristics of HCV and the COVID-19 virus as positive single-strand RNA viruses (+ssRNA), eleven FDA-approved HCV drugs and one RNA synthesis inhibitor antibiotic were specifically chosen to target the major protease (Mpro) of SARS-CoV-2. Various computational techniques were utilized to assess their physical and chemical properties as potential COVID-19 drugs, ultimately identifying all selected compounds as robust candidates warranting further experimental testing.

Methods

Selection of protein

The protein structure of “Structural and Active site analysis of SARS-CoV-2 Mpro complexed with N3 inhibitor (PDB ID: 6LU7) containing two chains (A&B)” was retrieved from the protein data bank (www.rcsb.org). The PDB ID of the protein 6LU7_A (Fig. 1) has a resolution of 2.16 Å [20], which is considered good quality for a protein structure, as a resolution of 2.0 Å or better is recommended. To avoid undesired molecular interactions during molecular docking and simulations, water molecules and unwanted complexes were removed from the downloaded protein structure.

The PROCHECK Ramachandran plot and ERRAT were used to validate the protein structure. The results indicate that there is one amino acid in the disallowed region, and 90.6% of residues are in the most favored region. A good quality model typically has >90% of amino acids in the most favored region [21]. ERRAT shows a quality factor of 96.552%, indicating that the protein structure is of



Fig. 1 Structural of SARS-CoV-2 Mpro (PDB ID: 6LU7_A)

high quality. A quality factor >50% is considered indicative of a good quality model [22]. Figure 2 illustrates the Ramachandran plot of 6LU7_A.

Ligand selection

We selected twelve FDA-approved drugs commonly used in the treatment of HCV, along with one RNA synthesis inhibitor antibiotic, to investigate their inhibitory activities against the main protease (Mpro) of SARS-CoV-2 with PDB ID: 6LU7. The drugs selected are Daclatasvir (DAC), Elbasvir (ELB), Glecaprevir (GLE), Grazoprevir (GRA), Ombitasvir (OMB), Paritaprevir (PAR), Pibrentasvir (PIB), Rifampicin (RIF), Sofosbuvir (SOF), Velpatasvir (VEL), Voxilaprevir (VOX), and Ledipasvir (LED). Remdesivir (REM), extensively used in COVID-19 patient treatment during the pandemic, was chosen as a standard to validate the selected ligands. The structures of these ligands were obtained from PubChem and ZINC 15 databases. Ligand preparation and energy minimization were conducted using the PyRx screening tool (23). The Universal Force Field (UFF) was employed for energy minimization of all ligands via Open Babel within the PyRx software, and subsequently, all ligands were converted to the PDB format. These optimized ligand structures were further converted to the PDBQT format suitable for molecular docking using the graphical user interface of PyRx.

Molecular docking of all compounds was performed using PyRx software with AutoDock Wizard [24, 25]. The protein structures provided by the AutoDock Wizard panel were utilized to generate the macromolecules for docking studies. During molecular docking, ligands were treated as flexible, while proteins were considered rigid. Grid parameters for docking were generated using the AutoGrid engine in PyRx, with the grid box dimensions set to $X=13.20$ Å, $Y=13.20$ Å and $Z=13.20$ Å, and the center of the grid box positioned at $X=-28.14$, $Y=13.20$, $Z=59.17$ to predict the amino acids of the protein interacting with the ligands (Table 1).

Molecular dynamic simulation

Desmond, Schrödinger LLC was used to run molecular dynamic simulations for 50 ns [26, 27]. Atom movements are usually computed over time using MD simulations through the integration of Newton's classical equation of motion [28, 29]. Using the Protein Preparation Wizard of Maestro, the receptor–ligand combination underwent complex optimization and minimization. Utilizing the System Builder tool, every system was set up. An orthorhombic box solvent model called Transferable Intermolecular Interaction Potential 3 Points (TIP3P) was selected. The OPLS 2005 force field was employed in the simulation [30]. Counter ions were added to neutralize the models. 50 mM of sodium chloride (NaCl)

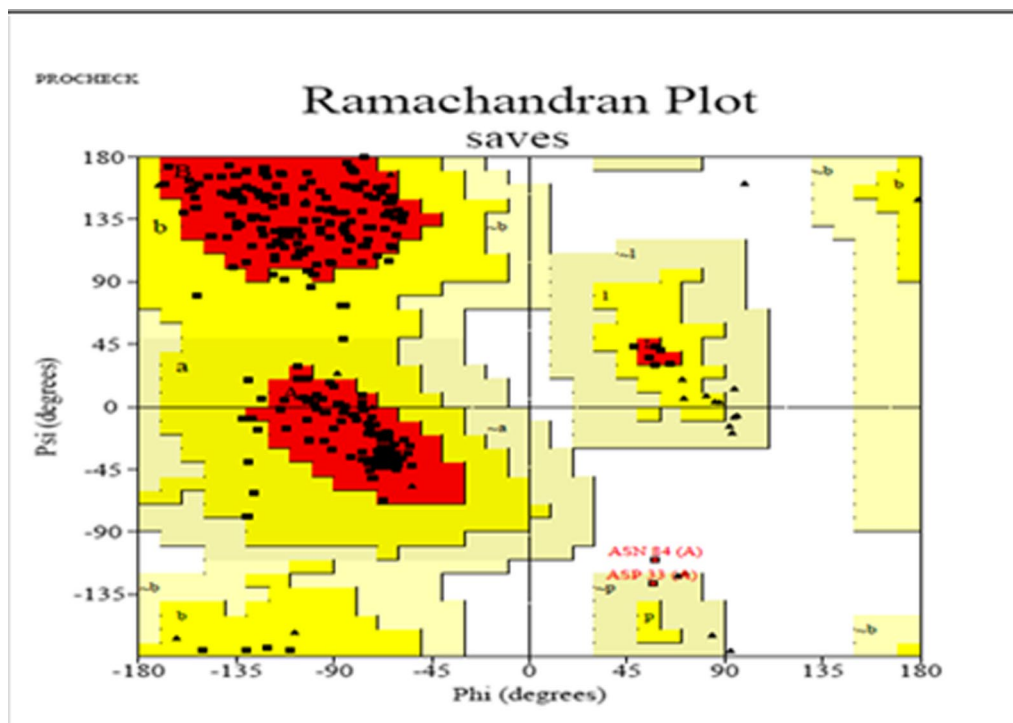


Fig. 2 Ramachandran plot of Mpro protein

Table 1 2D structural diagrams of selected ligands

Ligand name	Structure
1) Daclatasvir (DAC)	<p>The structure of Daclatasvir (DAC) features a central benzimidazole core. One nitrogen of the benzimidazole is substituted with a methyl group and a 1-methyl-2-(4-phenylphenyl)pyrrolidin-1-yl group. The other nitrogen is substituted with a methyl group and a 1-methyl-2-(4-phenylphenyl)pyrrolidin-1-yl group. The 2-position of the benzimidazole is substituted with a 1-methyl-2-(4-phenylphenyl)pyrrolidin-1-yl group. The 5-position of the benzimidazole is substituted with a 1-methyl-2-(4-phenylphenyl)pyrrolidin-1-yl group.</p>
2) Elbasvir (ELB)	<p>The structure of Elbasvir (ELB) features a central benzimidazole core. One nitrogen of the benzimidazole is substituted with a methyl group and a 1-methyl-2-(4-phenylphenyl)pyrrolidin-1-yl group. The other nitrogen is substituted with a methyl group and a 1-methyl-2-(4-phenylphenyl)pyrrolidin-1-yl group. The 2-position of the benzimidazole is substituted with a 1-methyl-2-(4-phenylphenyl)pyrrolidin-1-yl group. The 5-position of the benzimidazole is substituted with a 1-methyl-2-(4-phenylphenyl)pyrrolidin-1-yl group.</p>
3) Glecaprevir (GLE)	<p>The structure of Glecaprevir (GLE) features a central benzimidazole core. One nitrogen of the benzimidazole is substituted with a methyl group and a 1-methyl-2-(4-phenylphenyl)pyrrolidin-1-yl group. The other nitrogen is substituted with a methyl group and a 1-methyl-2-(4-phenylphenyl)pyrrolidin-1-yl group. The 2-position of the benzimidazole is substituted with a 1-methyl-2-(4-phenylphenyl)pyrrolidin-1-yl group. The 5-position of the benzimidazole is substituted with a 1-methyl-2-(4-phenylphenyl)pyrrolidin-1-yl group.</p>
4) Grazoprevir (GRA)	<p>The structure of Grazoprevir (GRA) features a central benzimidazole core. One nitrogen of the benzimidazole is substituted with a methyl group and a 1-methyl-2-(4-phenylphenyl)pyrrolidin-1-yl group. The other nitrogen is substituted with a methyl group and a 1-methyl-2-(4-phenylphenyl)pyrrolidin-1-yl group. The 2-position of the benzimidazole is substituted with a 1-methyl-2-(4-phenylphenyl)pyrrolidin-1-yl group. The 5-position of the benzimidazole is substituted with a 1-methyl-2-(4-phenylphenyl)pyrrolidin-1-yl group.</p>

Table 1 (continued)

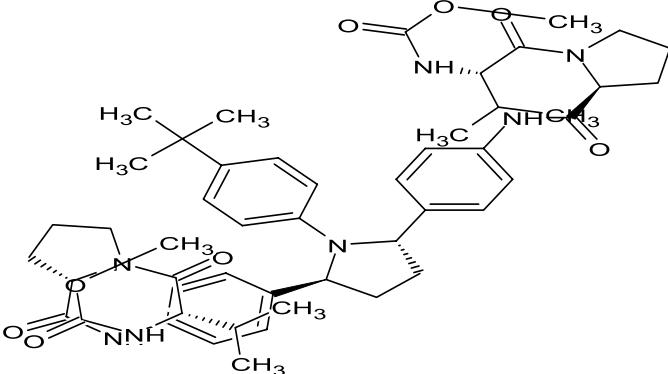
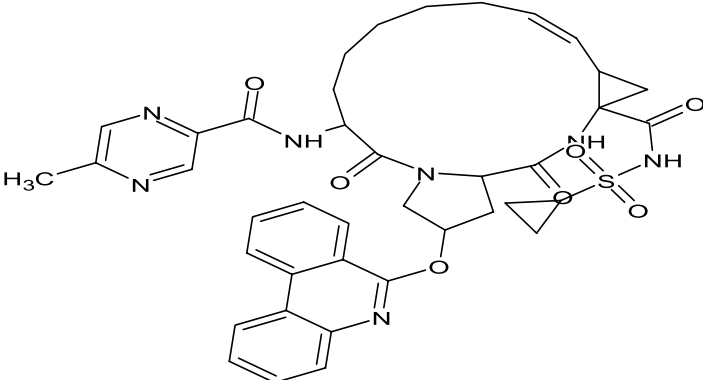
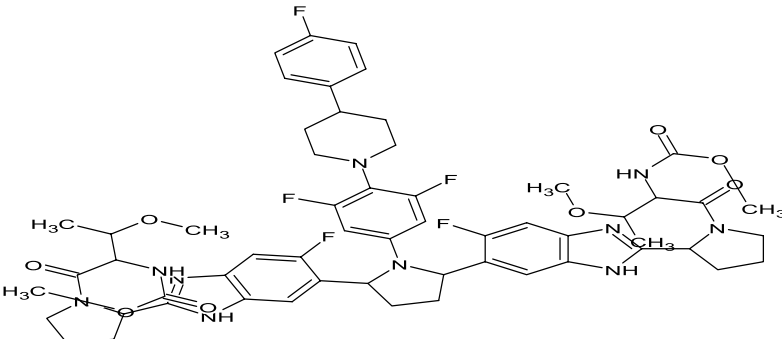
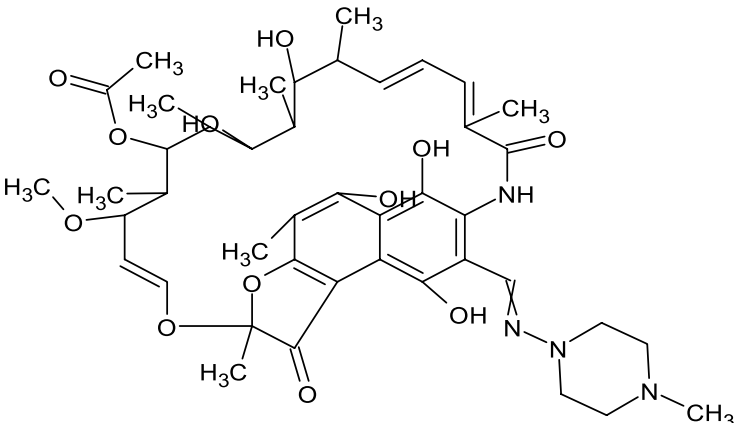
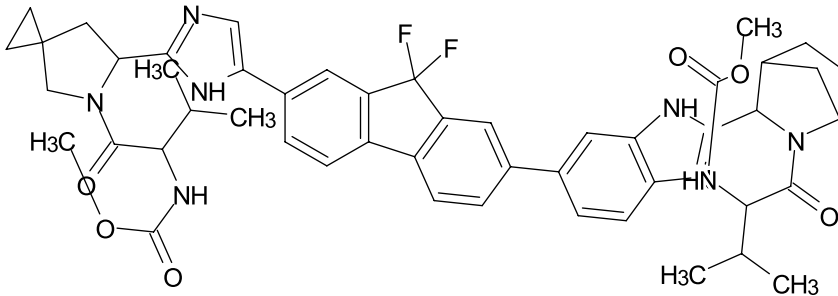
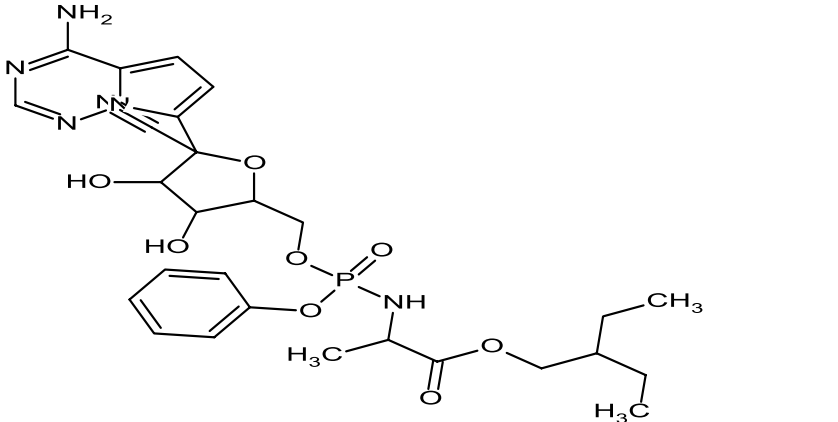
Ligand name	Structure
5) Ombitasvir (OMB)	
6) Paritaprevir (PAR)	
7) Pibrentasvir (PIB)	
8) Rifampicin (RIF)	

Table 1 (continued)

Ligand name	Structure
9) Sofosbuvir (SOF)	<p>The chemical structure of Sofosbuvir (SOF) is a nucleoside analog. It features a pyrimidine-2,4,6-trione ring system. The 5' carbon of the pyrimidine ring is linked to a ribose sugar moiety. The ribose sugar has a methyl group at the 2' position and a phosphonate group at the 3' position. The phosphonate group is further substituted with a methyl group and a methyl ester group. A phenyl ring is attached to the 4' carbon of the ribose sugar.</p>
10) Velpatasvir (VEL)	<p>The chemical structure of Velpatasvir (VEL) is a complex molecule. It consists of a central benzimidazole ring system. One of the benzimidazole nitrogens is substituted with a methyl group and a methoxy group. The other nitrogen is substituted with a methyl group and a methoxy group. The benzimidazole ring is linked to a benzene ring, which is further substituted with a methoxy group and a methyl group. The benzene ring is also linked to a pyridine ring, which is substituted with a methyl group and a methoxy group. The pyridine ring is further linked to a piperidine ring, which is substituted with a methyl group and a methoxy group.</p>
11) Voxilaprevir (VOX)	<p>The chemical structure of Voxilaprevir (VOX) is a large, complex molecule. It features a central piperidine ring system. The piperidine ring is substituted with a methyl group and a methoxy group. The piperidine ring is linked to a benzimidazole ring system, which is further substituted with a methyl group and a methoxy group. The benzimidazole ring is also linked to a benzene ring, which is substituted with a methyl group and a methoxy group. The benzene ring is further linked to a pyridine ring, which is substituted with a methyl group and a methoxy group. The pyridine ring is further linked to a piperidine ring, which is substituted with a methyl group and a methoxy group.</p>

Table 1 (continued)

Ligand name	Structure
12) Ledipasvir (LED)	
13) Remdesivir (REM)	

was supplied to replicate physiological circumstances. Throughout the simulation, the NPT ensemble with a temperature of 300 K and a pressure of 1 atm was selected. The models were relaxed before the simulation. The trajectories were stored for analysis at 100 ps intervals. The root-mean-square deviation (RMSD) of the protein and ligand over time was compared to ensure the stability of the simulation. Along with RMSD, root means square fluctuation (RMSF), solvent-accessible surface area (SASA), hydrogen bonds radius of gyration (Rg) and MM-GBSA values evaluated.

Results

There are 306 amino acid residues complexed with an inhibitor (N3-(N-[(5-Methylisoxazol-3-yl)Carbonyl])-Alanyl-L-Valyl-N, 1 (1r,2z) -4-(Benzyloxy) -4-Oxo-1-[(3r)-2-Oxopyrrolidin-3-yl]Methyl} But-2-Enyl)-L-Leucinamide) in the X-ray crystallographic structure of the SARS-CoV-2Mpro (PDB ID: 6LU7 Chain A) in Fig. 1. It consists of 23%, 31%, 45% and 28% α -helix, β -sheets, Coil and turns, respectively (36). According to X-ray diffraction, the protease had a resolution of 2.16. The structure has 87 hetero groups. The PROCHECK

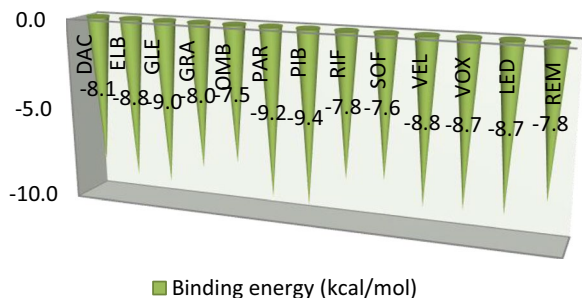
server has determined the R-values (free, work and observed) to be 0.235, 0.202 and 0.204, respectively.

Docking study

The Vina wizard has displayed nine possible binding positions as an output for each compound. The favorable binding affinity was estimated by finding the results of less than 1.0 Å in positional root-mean-square deviation (RMSD). The highest binding energy (most negative) was measured as the ligand with maximum binding affinity. The selected thirteen ligands efficiently bind to the main protease of SARS-CoV-2. The docking energies of all eleven ligands are shown in Table 2. From the docking analysis, all the selected ligands showed binding energy between -7.5 and -9.4 kcal/mol. PAR, GLE and PIB have been showing binding affinities against the main protease protein that were -9.2 , -9.0 and -9.4 kcal/mol, respectively.

The docking scores of DAC and ELB are -8.1 and -8.8 kcal, respectively. The residues of Mpro main chain interaction with the ligand are identified in Fig. 3. The DAC binds to the SARSCoV2 Mpro strongly, and the polar and non-polar amino acid residues involved are LYS5, TYR 126, LYS137, GLU290, ASP289,

Table 2 Binding energy values of docking analysis



^a All individuals coming within 1 m to inspect experimental setup and, in parentheses, all individuals that made attempts
^b Proportion successful

TYR239, LEU297 and TYR237. The molecular interaction is facilitated through hydrogen bond with residue TYR239, engages in Van der Waals interactions with GLU290, establishes pi-bonds with LYS5, ASP289, and GLU290, and creates alkyl bonds with TYR126, LYS137,

LYS5, TYR237, and LEU287. For ELB Amino acids PRO108, THR 196, GLU240, HIS246, GLN110, PRO293, ILE249 and PHE294 residues in the main protease were found in binding interaction with the ligand. The amino acid Hydrogen bond with THR196, GLN110 Van der Waals interactions with GLU290, pi-bond with PRO108, HIS246, PRO293, PHE284, ILE249, unfavored bond with GLU240.

Docking score of GLE and GRA is - 9.0 and - 8.0 kcal, respectively. The residues of Mpro main chain interaction with ligand are identified in Fig. 4. The GLE and SARS-CoV2 Mpro binding involves LYS137, VAL171, ALA194, ASP197, THR199, LEU286, LEU287 residues in main protease were found in binding interaction with the ligand. The amino acid forms hydrogen bond with LYS137, ASP197, halogen bond with LEU287, alkyl bond with VAL171, ALA194, LEU286, unfavored bond with THR199. The major protease’s HIS246, VAL202, GLN110, VAL297, PRO293, PRO252, PHE294 and VAL104 residues were discovered in the binding interaction with the ligand GRA. The amino acid forms

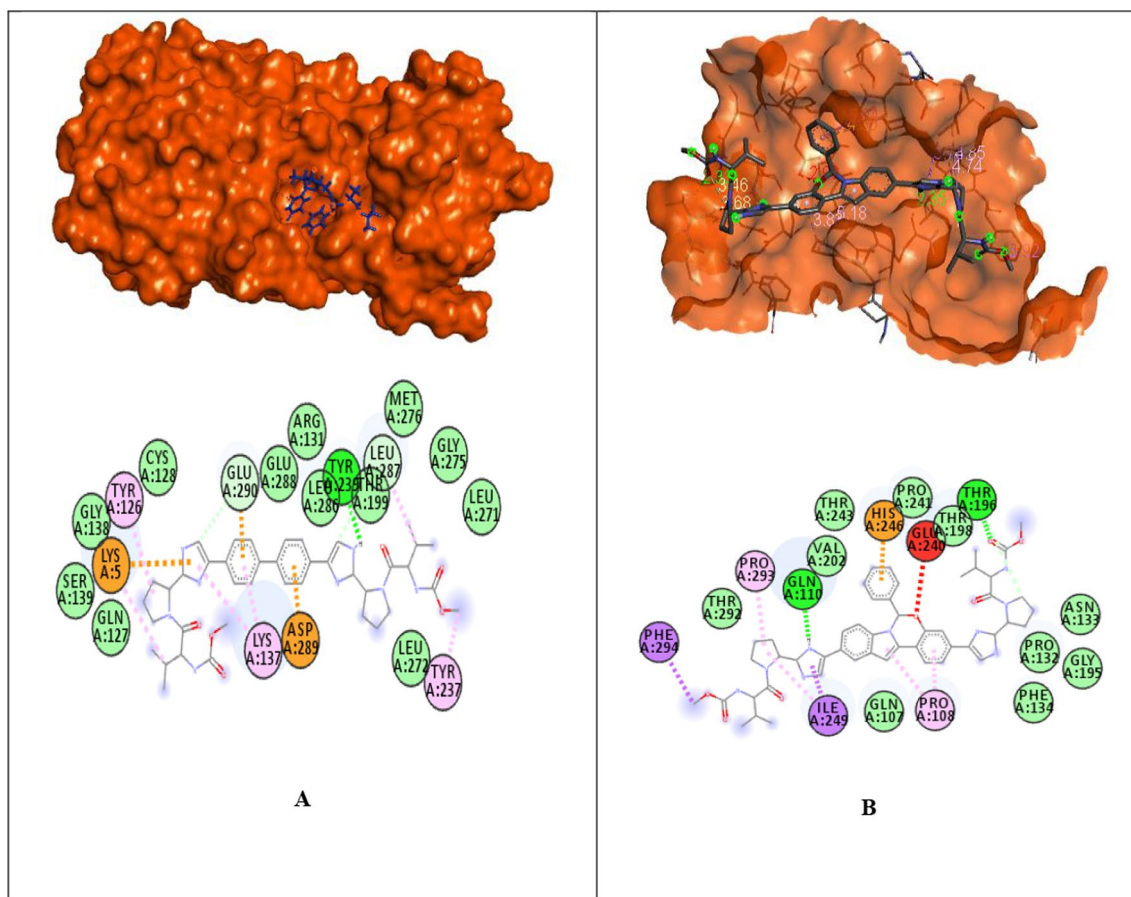


Fig. 3 a 3D and 2D ligand interaction diagram of DCA with SARS-CoV-2 Mpro; b 3D and 2D ligand interaction diagram of ELB with SARS-CoV-2 Mpro

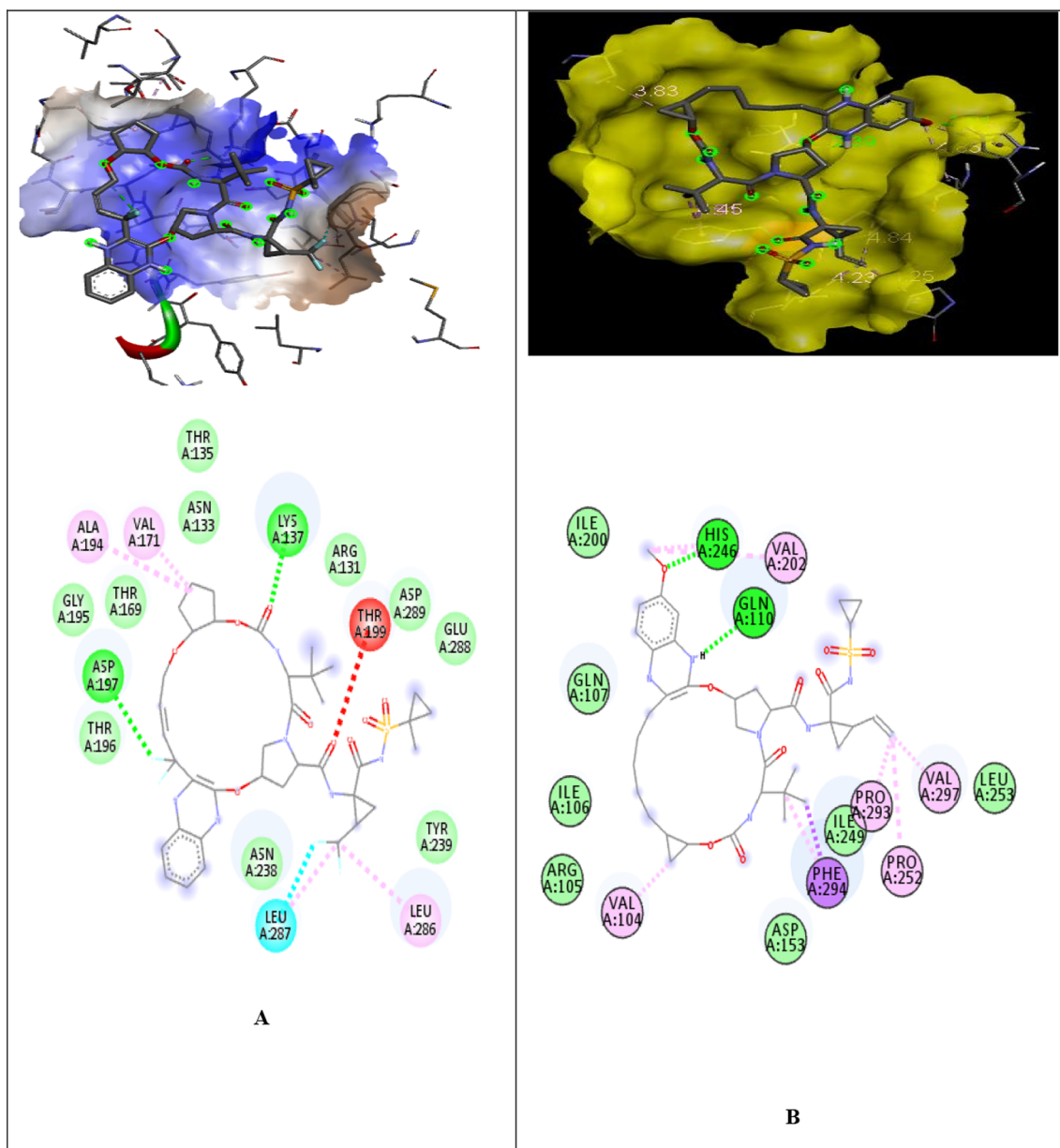


Fig. 4 a 3D and 2D ligand interaction diagrams GLE; b 3D and 2D ligand interaction diagrams GRA with SARS-CoV-2 Mpro

hydrogen bonds with HIS246 and GLN110, pi-sigma bonds with PHE294 and HIS246 and VAL202, VAL297, PRO252 and PRO293 form pi-alkaly bond.

Docking score of OMB is -7.5 kcal. The residues of Mpro main chain interaction with ligand are identified in Fig. 5. The amino acid forms hydrogen bonds with ASP197, carbon hydrogen bonds with LEU272, LYS137, Alkyl bonds with LEU287, LEU286, LEU 272 and VAL 171, Van der Waals bonds with LEU271, TYR237, GLN273, ASN274, GLY275.

The docking score of PAR is -9.2 kcal. The residues of Mpro main chain interaction with the ligand are identified in Fig. 6. VAL104, ASN151, GLN110, ILE249, PRO293, VAL202, HIS246, PRO252 and VAL297 residues in the main protease were found in binding interaction with the ligand. The amino acids have hydrogen bond with ASN151, VAL104, GLN110, pi-cation bond with HIS246, alkaly and pi-alkaly with VAL297, PRO252, PRO293, VAL202, ILE249, Van der

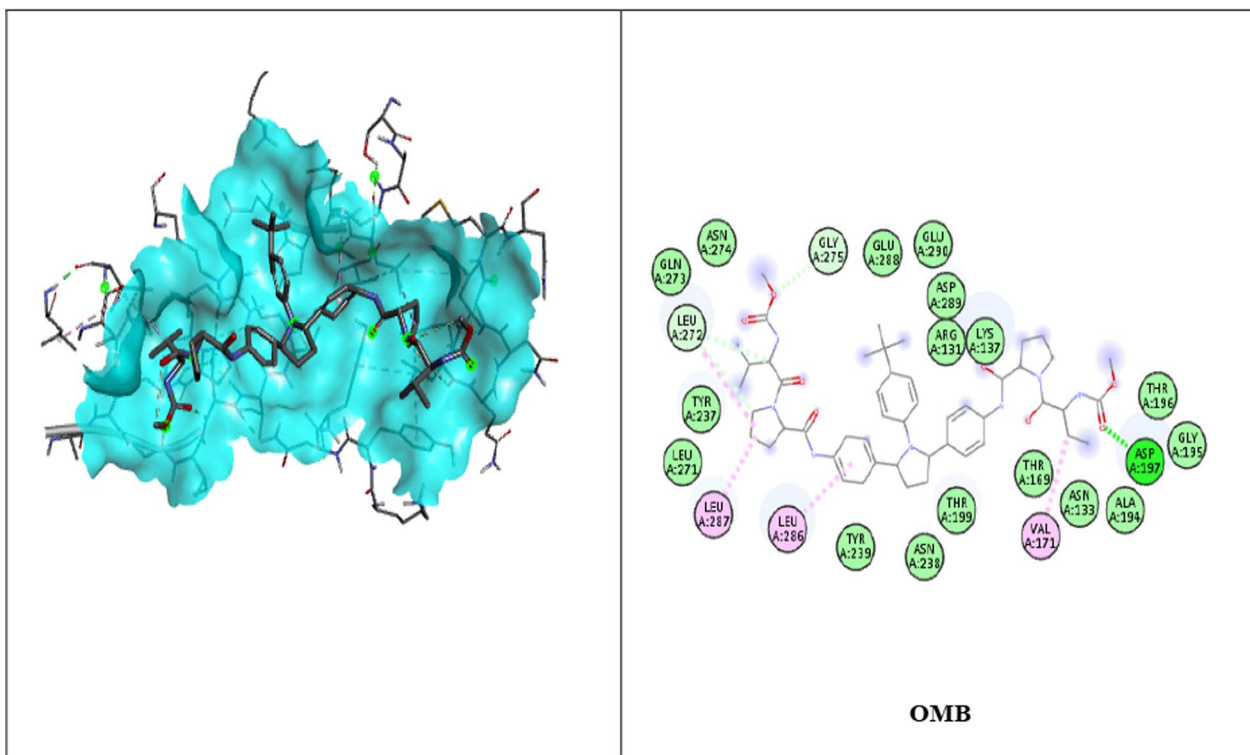


Fig. 5 3D and 2D ligand interaction diagrams of OMB with Mpro

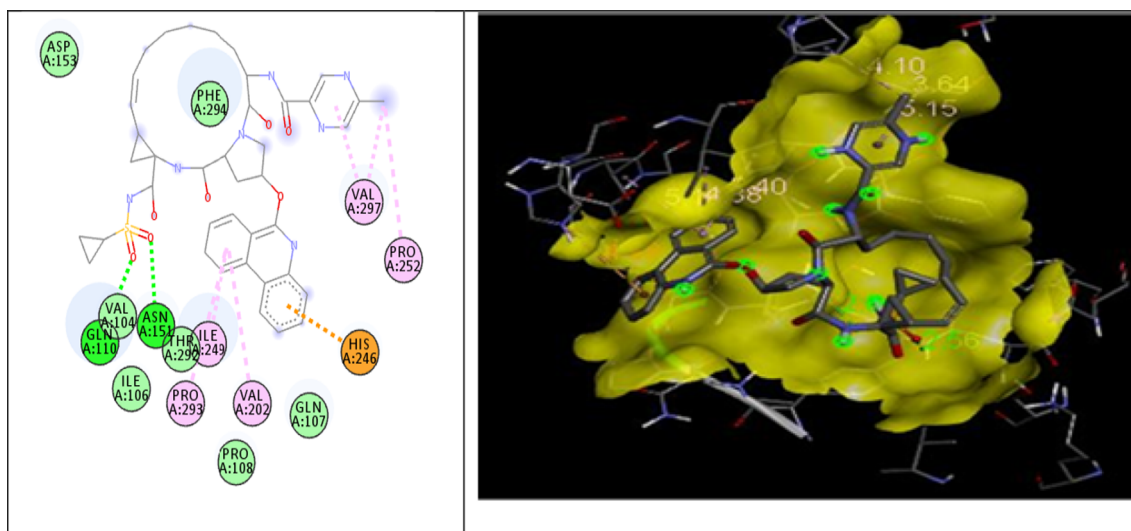


Fig. 6 2D and 3D ligand interaction diagrams of PAR with Mpro

Waals bond with ASP153, PHE294, THR292, ILE106, GLN107, ILE106, PRO108.

The docking score of PIB is – 9.4 kcal. The residues of Mpro main chain interaction with the ligand are identified in Fig. 7. LYS5, LYS137, ARG131, ASP289, LEU286, LEU287, ALA285, GLY278, MET276, ASN277, THR198,

ASP197, ALA193, ALA194 residues in main protease were found in binding interaction with the ligand. Figure 7 shows the ligand interaction diagrams of PIB with SARS-CoV-2 Mpro. The amino acids have hydrogen bond with ARG135, ALA285, GLY278, MET276, ASN277, ASP197, pi-cation bond with LYS5, LYS137,

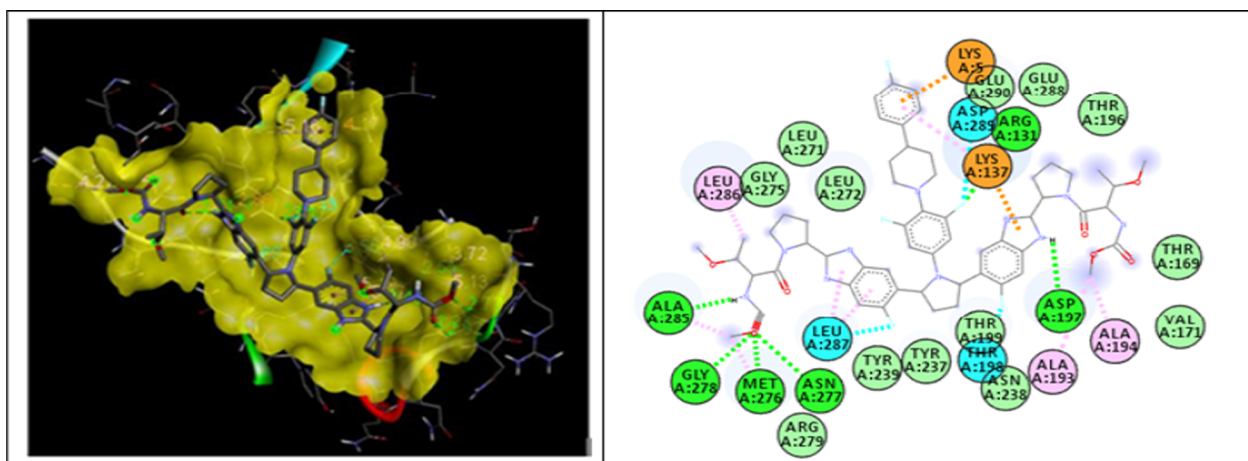


Fig. 7 3D and 2D ligand interaction diagrams of PIB with Mpro

halogen bond with ASP289, LEU287, THR198, alkyl and pi-alkyl with ALA193, ALA194, LYS137, LEU286, LEU287, MET276, ALA285, Van der Waals bond with LEU271, GLY275, LEU272, TYR239, TYR237, ASN238, VAL171, THR169, THR196, GLU288, GLU290.

The docking score of RIF is -7.8 kcal/mol. The residues of Mpro main chain interaction with the ligand are identified in Fig. 8. ASP153, SER158, GLN110, ILE249, PHE294, PHE8, VAL104 residues in the main protease were found in binding interaction with the ligand. The amino acids have hydrogen bond with GLN110, ASN151, PHE294, GLN107, SER158 alkyl and pi-alkyl with VAL104, ILE106, PRO293, pi-pi bond with PHE294, Van der Waals bond with LYS102, ASP153, VAL297, ILE249, PRO252, ARG105, THR292.

GLY275, LEU272, TYR239, TYR237, ASN238, VAL171, THR169, THR196, GLU288, GLU290.

The docking score of SOF is -7.6 kcal/mol. The residues of Mpro main chain interaction with the ligand are identified in Fig. 8. ILE106, ILE249, VAL297, GLN110, ASN151, ASP153, SER158 and PHE294 residues in the main protease were found in binding interaction with the ligand. The amino acids have hydrogen bond with GLN110, ASN151, PHE294, GLN107, SER158 alkyl and pi-alkyl with VAL104, ILE106, PRO293, pi-pi bond with PHE294, Van der Waals bond with LYS102, ASP153, VAL297, ILE249, PRO252, ARG105, THR292.

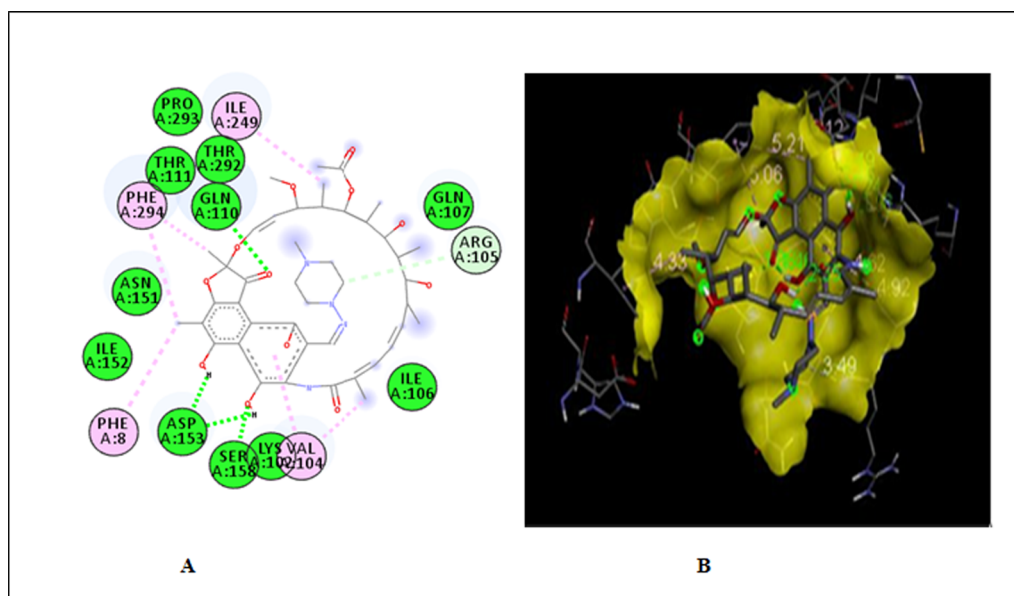


Fig. 8 a 2D ligand interaction diagram, b 3D interaction diagram of RIF with Mpro

The docking score of VEL is -8.8 kcal/mol. Main protease residues PRO132, HIS246, GLN110, VAL202, PRO241, PHE294, ILE106 and ILE249 were found in binding interaction with the ligand. The amino acids have hydrogen bond with PRO132, GLN110, alkyl and pi-alkyl with VAL202, ILE249, ILE106, PRO293, pi-pi bond with PHE294, pi-cation bond with HIS246, Van der Waals bond with ASN133, THR196, GLY195, ASP153, THR111, ASN151, VAL297, THR292, GLY109, ILE200, GLU240, PRO108, PHE134. The docking score of VOX is -8.7 kcal/mol. Residues in the main protease found in binding interaction with the ligand are ARG131, ASN238, THR199, LYS236, ASP197 and TYR237, and the amino acids have hydrogen bonds with ARG131, LYS236, ASN238, THR199 and pi-alkyl bond with TYR237. Van der Waals and halogen bonds were also observed. Figure 9 shows interaction diagrams of VEL & VOX with SARS-CoV-2 Mpro.

The docking score of LED is -8.7 kcal/mol. The residues of Mpro main chain interaction with the ligand are identified in Fig. 10. Conventional hydrogen bonds with ALA285, MET276, ASN277, GLY170, TYR239, pi-cation bond with LYS137, pi donor hydrogen bond with LEU287, pi-alkyl bonds with LEU286, HIS172, alkyl bond with LEU272, halogen bond with GLU288, ASP289 and Van der Waals bond with VAL171, LEU287, THR189, LU281 and carbon hydrogen bonds with protein amino acids.

The docking score of REM is -7.8 kcal/mol. The residues of Mpro main chain interaction with the ligand are identified in Fig. 10. Conventional hydrogen bonds with AGR188, THR190, HIS 41, pi-pi bond with HIS 41, pi-alkyl bonds with MET49, MET165 and Van der Waals and carbon hydrogen bonds with protein amino acids.

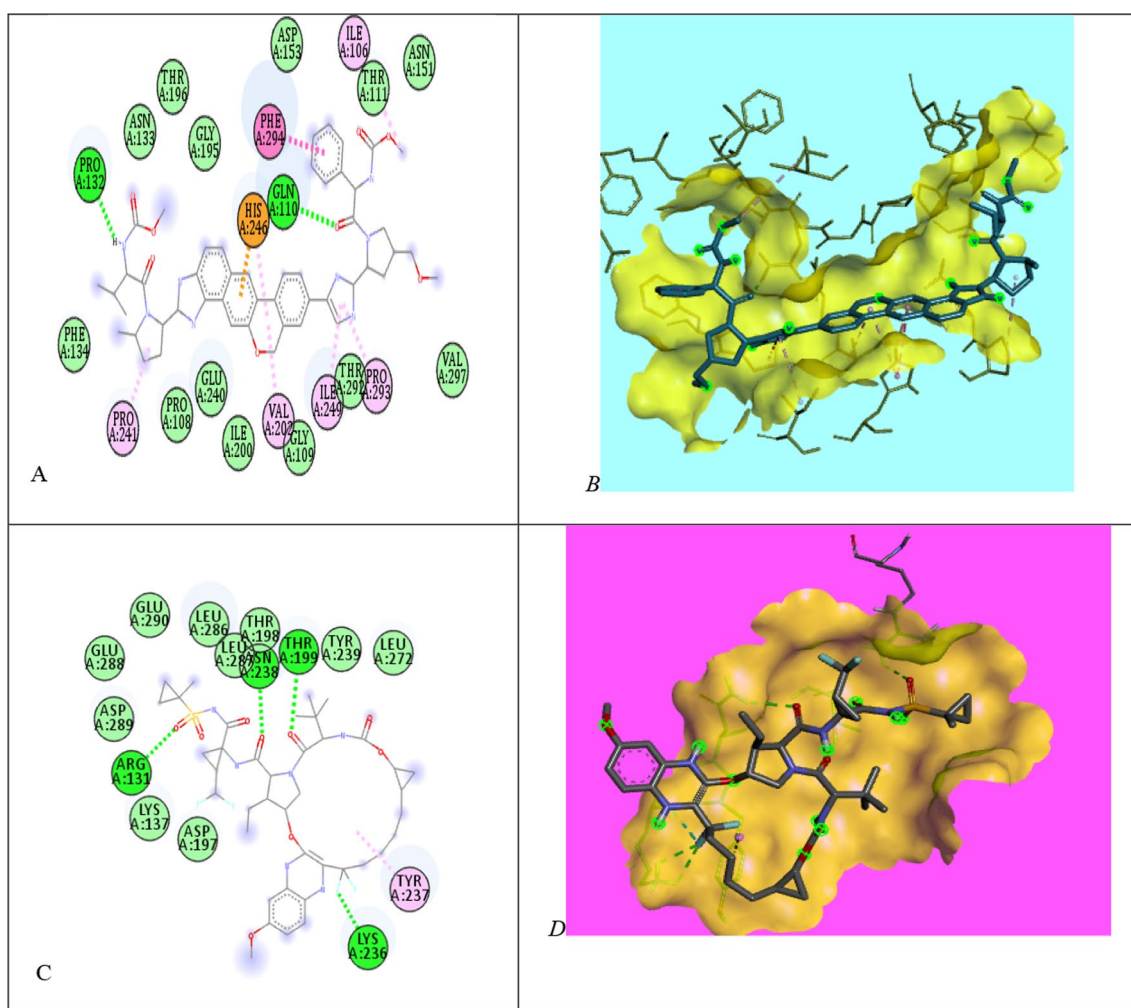


Fig. 9 a, c 2D ligand interaction diagrams and b, d 3D interaction diagrams of VEL & VOX with Mpro

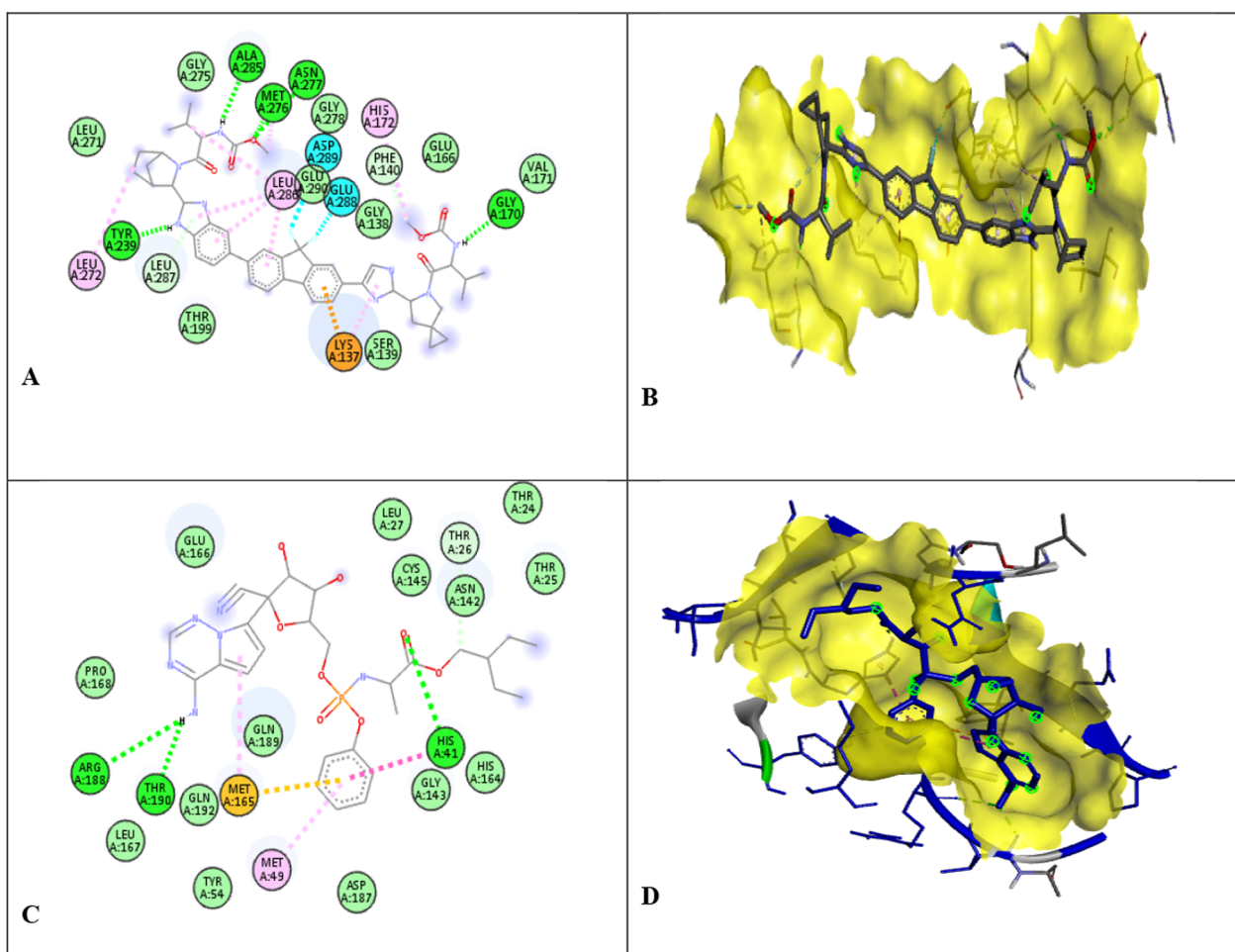


Fig. 10 a, c 2D ligand interaction diagram, b, d 3D ligand interaction diagrams of LED & REM with Mpro

Discussion

RMSD

The root-mean-square deviation (RMSD) is used to measure the average change in displacement of a selection of atoms for a particular frame with respect to a reference frame. It is calculated for all frames in the trajectory. The RMSD for frame x is:

$$\text{RMSD}_x = \sqrt{\frac{1}{N} \sum_{i=1}^N (r'_i(t_x) - r_i(t_{\text{ref}}))^2} \quad (1)$$

When comparing a protein's initial structural conformation to its final position, the difference between the backbones of the protein is measured using the root-mean-square deviation (RMSD). RMSD calculation was done for the entire C- α atom from the starting structures, which was considered an essential criterion to calculate the convergence of the protein–ligand complex system involved in the study. The stability of the complex was

demonstrated by the time-dependent variation in RMSD values for C-alpha atoms in ligand-bound proteins. Figures 11, 12 and 13 show the RMSD graphs of protein–ligand complexes. The complexes stabilized at 30 ns, according to the RMSD plots. On the other hand, at 30 ns, the RMSD of the protein-bound ligand increased slightly. This flip might be the result of a conformational shift in the ligand's rotatable bonds.

RMSF

RMSF stands for root-mean-square fluctuation. This numerical measurement is similar to RMSD, but instead of indicating positional differences between entire structures over time, RMSF calculates the flexibility of individual residues—the extent to which a particular residue moves (fluctuates) during a simulation. RMSF per residue is typically plotted against residue number and can indicate which amino acids in a protein contribute most to molecular motion. Analysis of residue fluctuation reveals that RMSF values for all complex structures followed

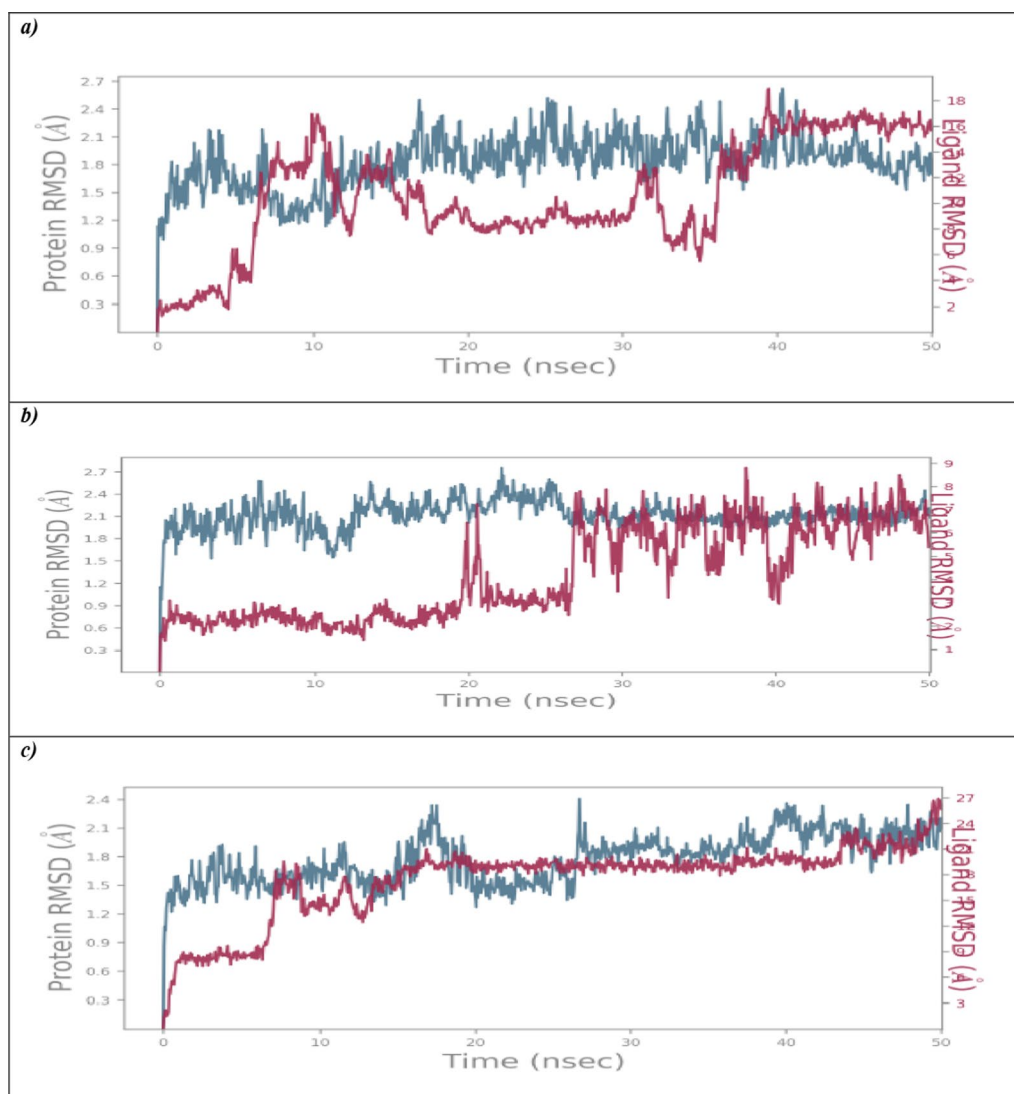


Fig. 11 Root-mean-square deviation (RMSD) overlay between free protein before docking and protein after docking with **a** DAC, **b** ELB and **c** GLE, respectively

a similar pattern. Notably, residues with higher fluctuations were observed between positions 100 and 306. Overall, the graph suggests that the 6LU7-PAR complex exhibited higher fluctuations during the final simulation period compared to all other complexes. Additionally, the average RMSF values across all complexes range from 0.4 to 4.8, except for the 6LU7-PIB complex, where RMSF values fluctuated from 0.8 to 6.4. See Fig. 14 for RMSF graphs.

Solvent-accessible surface area

Solvent-accessible surface area (SASA) is defined as the surface area of a protein that interacts with solvent molecules [22]. SASA is considered a pivotal element

in investigations regarding protein stability and folding, characterized by its theoretical center within the solvent sphere and exhibiting van der Waals interactions with the molecular surface. Average SASA values for all complexes were monitored during 50 ns MD simulations. The average SASA values for all 6LU7-ligand complexes ranged from 14,500 to 15,500 Å², respectively. No major changes were observed in SASA values due to ligand binding. See Fig. 15 for SASA graphs.

Radius of gyration (RoG)

The radius of gyration measures the compactness of a protein structure, which reflects its stability. The greater the fluctuation, the less stable the structure. Therefore, it

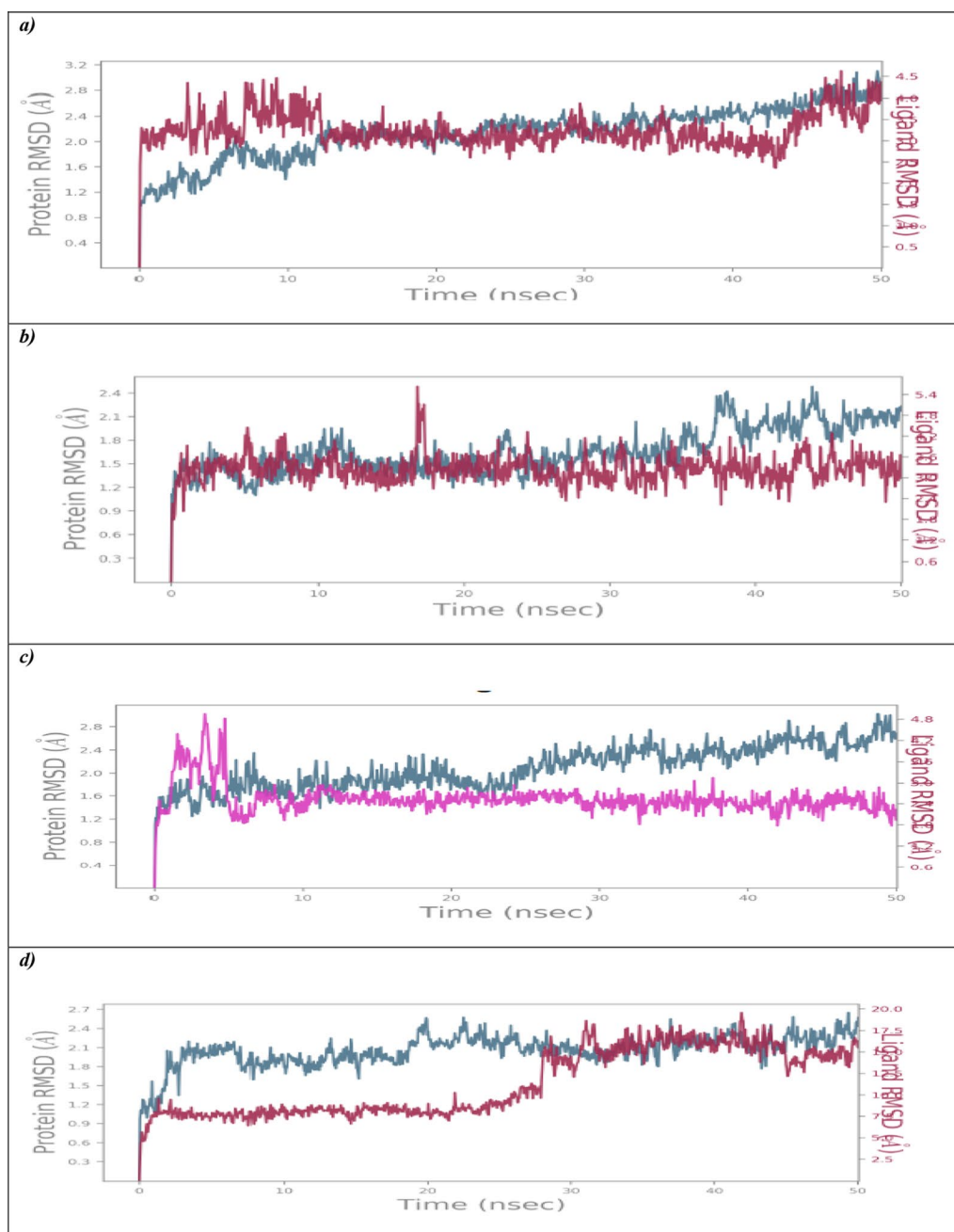


Fig. 12 Root-mean-square deviation (RMSD) overlay between free protein before docking and protein after docking with **a** GRA, **b** LED, **c** OMB and **d** PAR, respectively

plays a significant role in comparative studies. The stability of protein–ligand complexes was analyzed in terms of RoG over a 50-ns simulation period. The average Rg was found to be 21–23 nm for all protein–ligand complexes with a % RSD of 0.05. The minimal standard deviation values indicate that ligand binding to the protein’s active site does not induce major conformational changes in the protein structure. This suggests that all protein–ligand

complexes remained stable throughout the entire simulation period. See Fig. 16 for radius of gyration (RoG) plots of selected ligands with the protein.

Hydrogen bond

Hydrogen bonds are crucial for ligand binding. Their properties significantly influence drug specificity, metabolism and absorption, making them essential

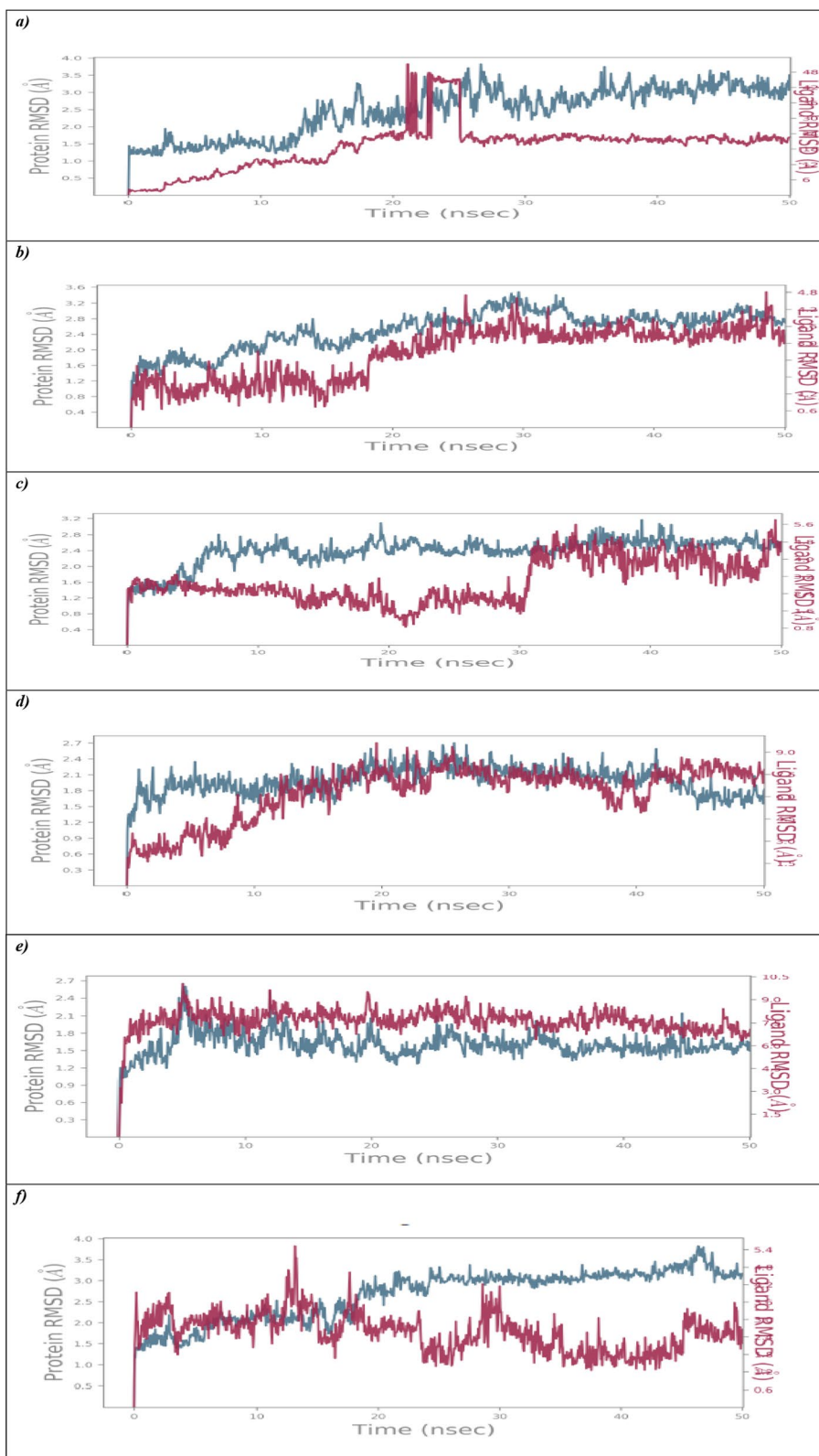


Fig. 13 Root-mean-square deviation (RMSD) overlay between free protein before docking and protein after docking with **a** PIB, **b** RIF, **c** SOF, **d** VEL, **e** VOX and **f** REM, respectively

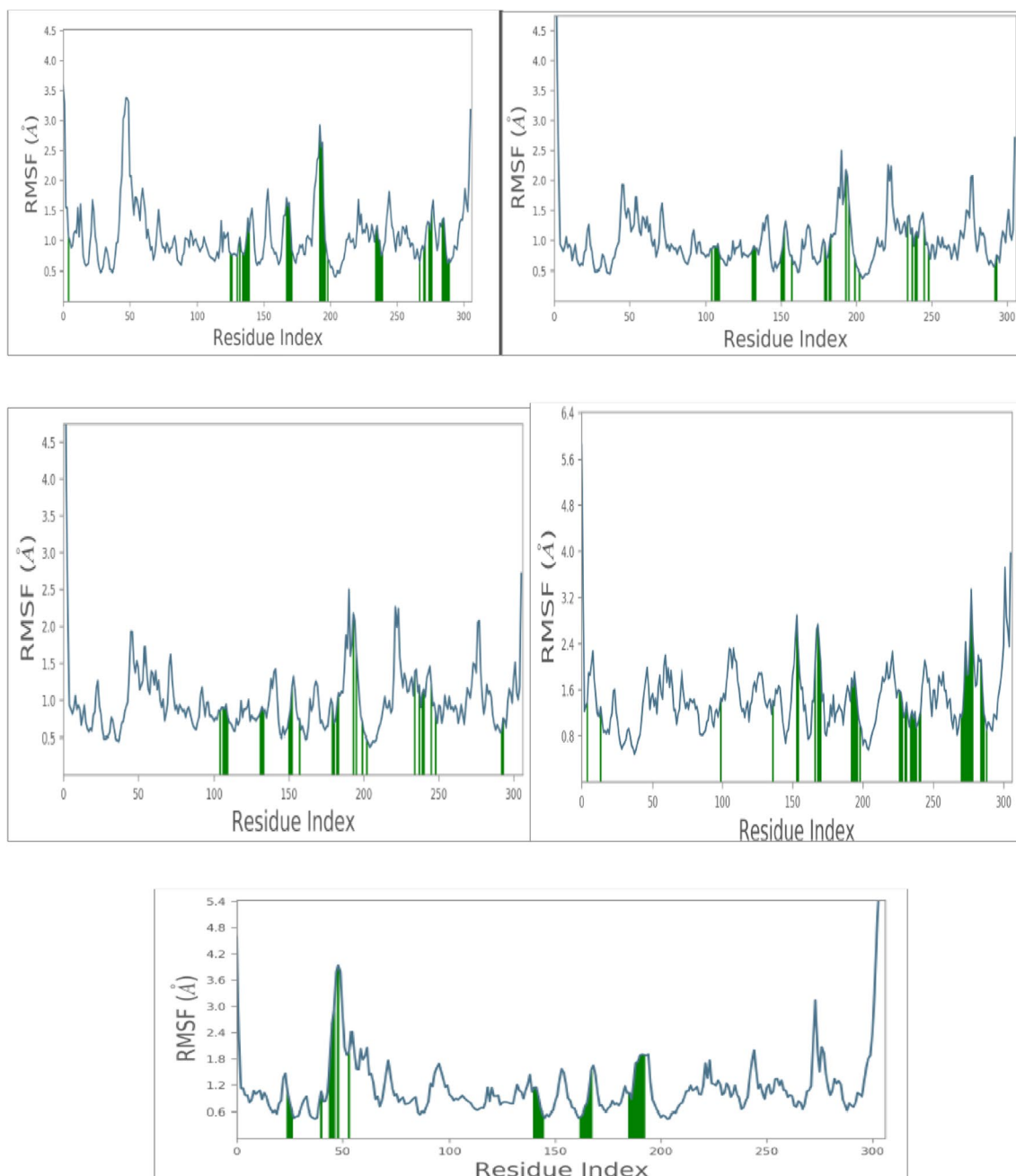


Fig. 14 Root-mean-square fluctuation (RMSF) of the target protein residues complexes with the selected ligand DAC, ELB, GLE, PIB & REM, respectively

considerations in medication design. Four subtypes of hydrogen bonds can be distinguished between a protein and a ligand: side-chain donor, side-chain acceptor and backbone acceptor.

The most important interactions between ligands and the protein consisted of hydrogen bonds, as shown in Fig. 16. Various amino acid residues were found to participate in hydrogen bonding. Additionally, the

ligand–protein interaction was carefully monitored throughout the simulation analysis process. H-bonds, hydrophobic interactions, ionic interactions and water bridges are examples of molecular contacts that demonstrate the connection between the target protein and the chosen ligand. The interaction of the ligand along the x-axis was determined for every frame of the trajectory. Furthermore, distinct interactions with the ligand, such

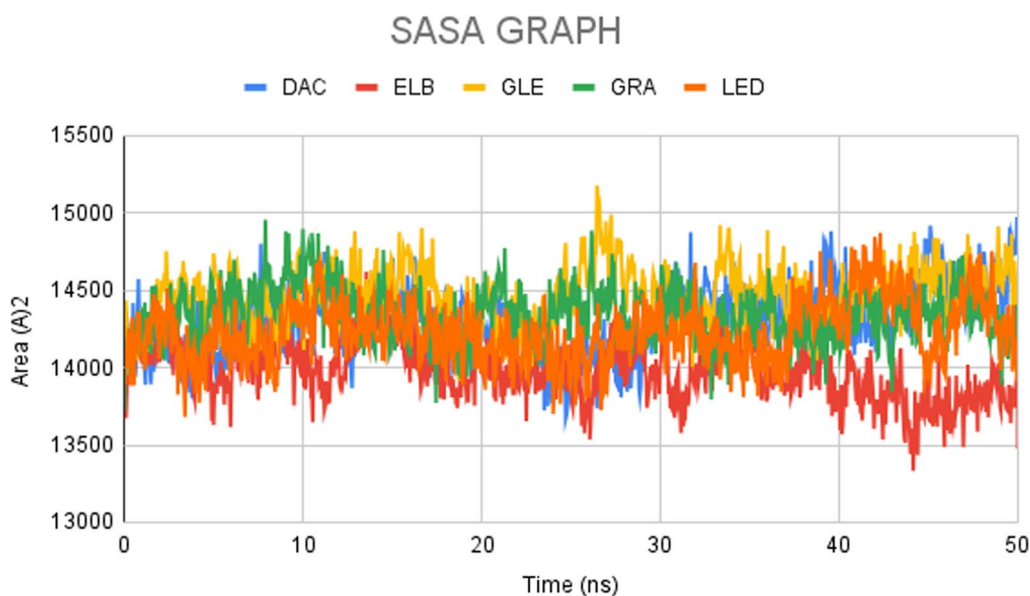


Fig. 15 SASA graphs of selected ligands

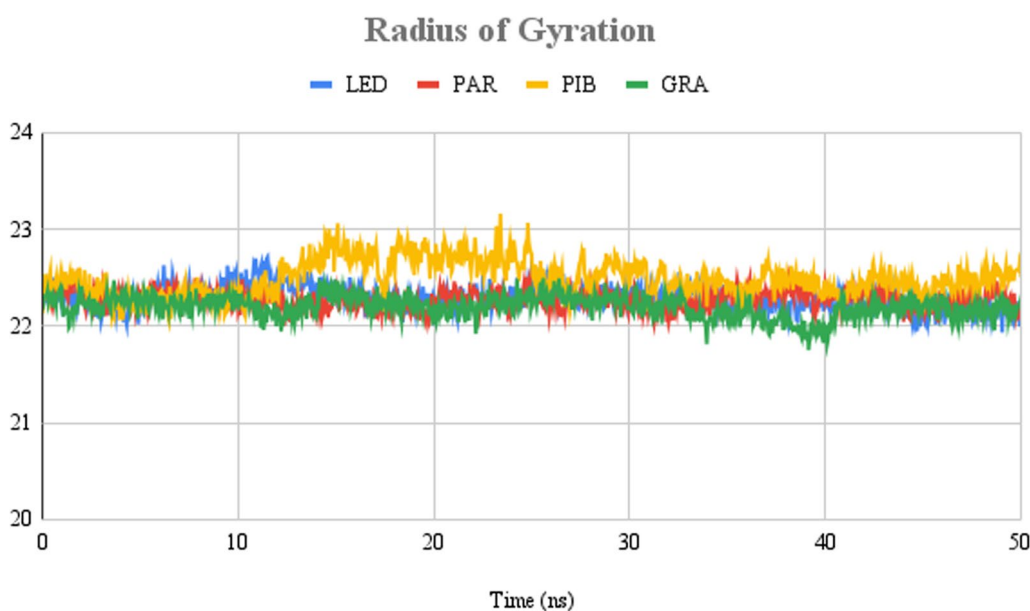


Fig. 16 Radius of gyration (RoG) plots of ligands with protein

as hydrophobic interactions, ionic interactions and water bridges, were observed. The protein–ligand heat map is shown in Fig. 17.

A timeline representation of the interactions and contacts (H-bonds, hydrophobic, ionic, water bridges) is summarized in the previous page. The top panel shows the total number of specific contacts the protein makes

with the ligand over the course of the trajectory. The bottom panel shows which residues interact with the ligand in each trajectory frame. Some residues make more than one specific contact with the ligand, which is represented by a darker shade of orange, according to the scale to the right of the plot. For all twelve protein–ligand complexes the protein–ligand contact heat map generated and verified the interactions and contacts.

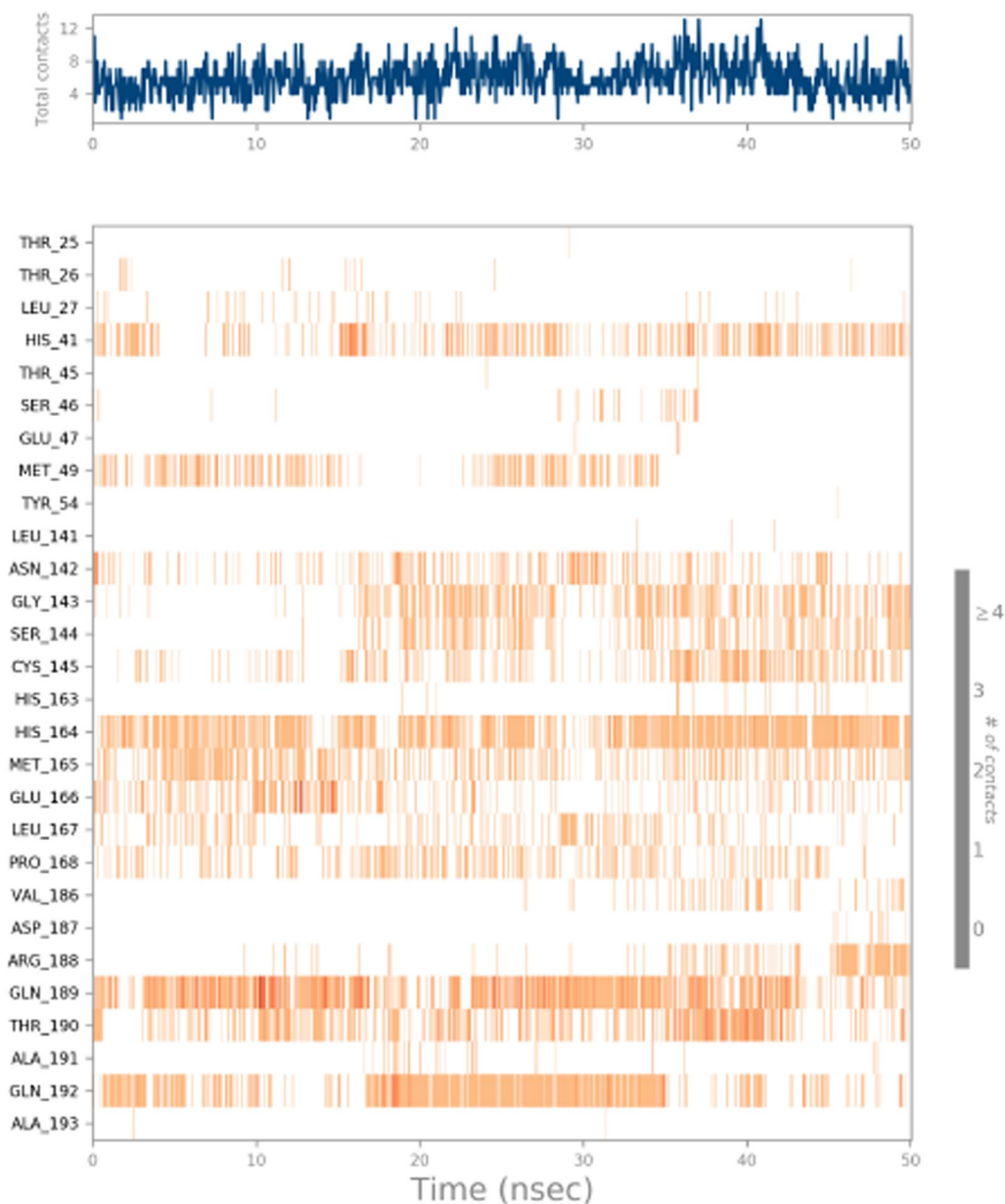


Fig. 17 Protein–ligand contact heat map throughout trajectory (protein-REM complex)

Protein–ligand contact

Throughout the simulation, it is possible to observe how the ligand and protein interact. As the above plot illustrates, these interactions can be type-categorized and summarized. There are four different forms of protein–ligand interactions, or “contacts”: hydrophobic, ionic, water bridge and hydrogen bonding. The ‘Simulation Interactions Diagram’ panel allows for the exploration of more detailed subtypes within each interaction type. Over the trajectory, the stacked bar

charts undergo normalization. Figure 18 shows the protein ligand contact bar diagram.

Molecular mechanics and generalized born surface area (MM-GBSA) calculations

The molecular mechanics generalized Born surface area (MM-GBSA) module of prime was used to determine the binding free energy (G_{bind}) of docked complex during MD simulations of Mpro complexed with selected ligands. Using the OPLS 2005 force field, VSGB solvent

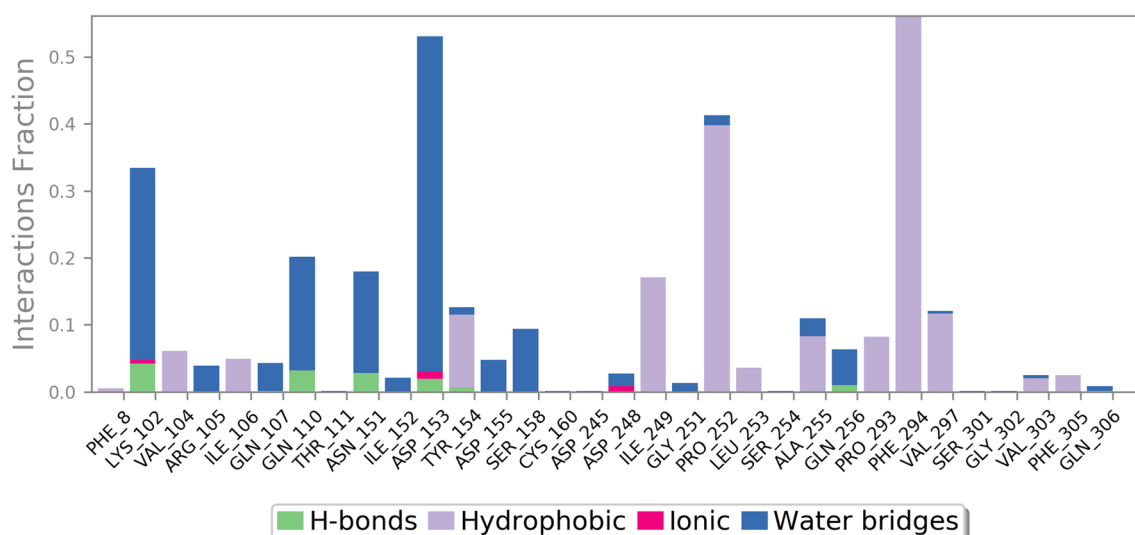


Fig. 18 Protein–ligand contact bar diagram of trajectory (protein-PAR complex)

Table 3 MM/GBSA binding free energy values

Name of the ligand	MMGBSA (k/cal)
DAC	− 76.828827
ELB	− 66.272588
GRA	− 47.941362
GLE	− 22.378531
LED	− 57.653165
PAR	− 34.390086
SOF	− 47.638993
RIF	− 54.152987
VEL	− 67.841531
VOX	− 91.610103
OMB	− 57.034641
REM	− 73.094995
PIB	0.064481

model and rotamer search techniques, the binding free energy was estimated. The MD trajectory frames were chosen at intervals of 10 ns after the MD run. The total free energy binding was calculated using Eq. 2:

$$dG_{\text{bind}} = G_{\text{complex}} - (G_{\text{protein}} + G_{\text{ligand}}) \quad (2)$$

where dG_{bind} =binding free energy, G_{complex} =free energy of the complex, G_{protein} =free energy of the target protein and G_{ligand} =free energy of the ligand. Table 3 shows the MMGBSA values of protein–ligand complexes.

Table 4 presents that most of the selected ligands exhibit favorable free energy of binding values compared to Remdesivir, which was used as the reference compound. Among the 12 selected compounds (GLE, PAR,

PIB, VEL, ELB), those with docking scores ≥ -8.8 kcal/mol against SARS-CoV-2 Mpro were identified. These complexes were subsequently analyzed for intermolecular interactions, complex stability, and binding affinity relative to the SARS-CoV-2 Mpro-REM reference complex using computational methods. Based on comprehensive analysis, GLE, PAR, PIB, VEL, and ELB were found to establish strong molecular contacts within the active site of SARS-CoV-2 Mpro. Therefore, these compounds are potential candidates for further evaluation as SARS-CoV-2 Mpro inhibitors through in vitro studies, with the goal of repurposing them for treatment against SARS-CoV-2 infection.

Conclusion

This study employed molecular docking methods to screen FDA-approved compound databases, utilizing FDA-approved HCV drugs and an RNA synthesis inhibitor antibiotic. The objective was to identify molecules within these substances that could effectively inhibit COVID-19 by targeting the main protease (Mpro). The selected ligands exhibited promising COVID-19 inhibition, as indicated by improved energy scores using the blind docking approach. Subsequently, molecular dynamics (MD) simulations were conducted over 50 ns (ns) using Desmond, Schrödinger LLC software, to further evaluate the chosen compounds in their best docking poses. Additionally, various parameters including RMSD, RMSE, Rg, SASA and MMGBSA were calculated. Our data suggest that these findings support the repurposing of existing pharmacological molecules for the treatment of additional diseases during urgent pandemic situations such as COVID-19.

Table 4 Binding energy and active site residues present in Mpro(6LU7)-ligand complex

Ligand	Predicted free energy of binding (ΔG) kcal/mol	Amino acid residues involved in bonds
Daclatasvir (DAC)	- 8.1	LYS5, TYR 126, LYS137, GLU290, ASP289, TYR239, LEU297, TYR237
Elbasvir (ELB)	- 8.8	PRO108, THR 196, GLU240, HIS246, GLN110, PRO293, ILE246, PHE294
Glecaprevir (GLE)	- 9.0	VAL171, ALA194, THR196, TYR239, LUE286, ARG131, LYS137, ASP197, THR199, ASN238, ASP289
Grazoprevir (GRA)	- 8.0	HIS246, VAL202, GLN110, VAL297, PRO293, PRO252, PHE294, VAL104, GILE249, GLN107, ILE106, LEU253, ASP153
Ombitasvir (OMB)	- 7.5	ASP197, LEU272, LYS137, LEU287, LEU286, VAL 171, LEU271, TYR237, GLN273, ASN274, GLY275
Paritaprevir (PAR)	- 9.2	VAL104, ASN151, GLN110, ILE249, PRO293, VAL202, HIS246, PRO252, VAL29, ASP153, PHE294, THR292, ILE106, GLN107, PRO108
Pibrentasvir (PIB)	- 9.4	LYS5, LYS137, ARG131, ASP289, LEU286, LEU287, ALA285, GLY278, MET276, ASN277, THR198, ASP197, ALA193, ALA194, LEU271, GLY275, LEU272, TYR239, TYR237, ASN238, VAL171, THR169, THR196, GLU288, GLU290
Rifampicin (RIF)	- 7.8	ASP153, SER158, GLN110, ILE249, PHE294, PHE8, VAL104, LEU271, GLY275, LEU272, TYR239, TYR237, ASN238, VAL171, THR169, THR196, GLU288, GLU290
Sofosbuvir (SOF)	- 7.6	ILE106, ILE249, VAL297, GLN110, ASN151, ASP153, SER158, PHE29, LYS102, ASP153, VAL297, ILE249, PRO252, ARG105, THR292
Velpatasvir (VEL)	- 8.8	PRO132, HIS246, GLN110, VAL202, PRO241, PHE294, ILE106, ILE249, ASN133, THR196, GLY195, ASP153, THR111, ASN151, VAL297, THR292, GLY109, ILE200, GLU240, PRO108, PHE134
Voxilaprevir (VOX)	- 8.7	ARG131, ASN238, THR199, LYS236, ASP197, TYR237, ASP289, GLU290, LEU286, THR198, LEU272, GLU288, ASP289, LYS137, LEU289
Ledipasvir (LED)	- 8.7	ALA285, MET276, ASN277, GLY170, TYR239, LYS137, LEU287, LEU286, HIS172, LEU272, GLU288, ASP289, VAL171, LEU287, THR189, LU281
Remdesivir (REM)	- 7.8	AGR188, THR190, HIS 41, MET49, MET165, GLU166, LEU27, CYS145, HIS164, LEU167, GLN189, PRO168

Acknowledgements

The authors would like to be thankful to Andhra University authorities and colleagues of School of Chemistry, Andhra University.

Author contributions

MVK helped in conceptualization, experimentation and writing original draft and editing; TS was involved in supervision, formal analysis, review; and GND contributed to conceptualization, experimentation and writing original draft. All the authors read the manuscript and approved.

Funding

Not applicable.

Availability of data and materials

The datasets analyzed during the current study are not publicly available due to confidentiality but are available from the corresponding author on reasonable request.

Declarations**Ethics approval and consent to participate**

Not applicable.

Consent for publication

Not applicable.

Competing interests

The authors declare that they have no competing interest.

Received: 30 January 2024 Accepted: 14 August 2024

Published online: 09 September 2024

References

- Hui D, Azhar IE, Madani TA, Ntoumi F, Kock R, Dar O, Ippolito G, Mchugh TD, Memish ZA, Drosten C, Zumla A, Petersen E (2020) The continuing 2019-nCoV epidemic threat of novel coronaviruses to global health—the latest 2019 novel coronavirus outbreak in Wuhan, China. *Int J Infect Dis IJID Off Publ Int Soc Infect Dis* 91:264–266. <https://doi.org/10.1016/j.ijid.2020.01.009>
- Li Z, Wu M, Yao J, Guo J, Liao X, Song S, Yan J (2020) Caution on kidney dysfunctions of COVID-19 patients. <https://doi.org/10.1101/2020.02.08.20021212>
- Enayatkhani M, Hasaniazad M, Faezi S, Gouklani H, Davoodian P, Ahmadi N, Ahmadi K (2021) Reverse vaccinology approach to design a novel multi-epitope vaccine candidate against COVID-19: an in silico study. *J Biomol Struct Dyn* 39(8):2857–2872. <https://doi.org/10.1080/07391102.2020.1756411>
- Kandwal S, Fayne D (2022) Repurposing drugs for treatment of SARS-CoV-2 infection: computational design insights into mechanisms of action. *J Biomol Struct Dyn* 40(3):1316–1330. <https://doi.org/10.1080/07391102.2020.1825232>
- Pant S, Singh M, Ravichandiran V, Murty USN, Srivastava HK (2021) Peptide-like and small-molecule inhibitors against Covid-19. *J Biomol Struct Dyn* 39(8):2904–2913. <https://doi.org/10.1080/07391102.2020.1757510>

6. Furuta Y, Gowen BB, Takahashi K, Shiraki K, Smee DF, Barnard DL (2013) Favipiravir (T-705), a novel viral RNA polymerase inhibitor. *Antiviral Res* 100(2):446–454. <https://doi.org/10.1016/j.antiviral.2013.09.015>
7. Harrison C (2020) Coronavirus puts drug repurposing on the fast track. *Nat Biotechnol* 38(4):379–381. <https://doi.org/10.1038/d41587-020-00003-1s>
8. Wang M, Cao R, Zhang L, Yang X, Liu J, Xu M, Xiao G (2020) Remdesivir and chloroquine effectively inhibit the recently emerged novel coronavirus (2019-nCoV) in vitro. *Cell Res* 30(3):269–271. <https://doi.org/10.1038/s41422-020-0282-0>
9. Xu Z, Shi L, Wang Y, Zhang J, Huang L, Zhang C, Wang F-S (2020) Pathological findings of COVID-19 associated with acute respiratory distress syndrome. *Lancet Respir Med* 8(4):420–422. [https://doi.org/10.1016/S2213-2600\(20\)30076-X](https://doi.org/10.1016/S2213-2600(20)30076-X)
10. Khaerunnisa S, Kurniawan H, Awaluddin R, Suhartati S, Soetjipto S (2020) Potential inhibitor of COVID-19 main protease (Mpro) from several medicinal plant compounds by molecular docking study. <https://doi.org/10.20944/preprints202003.0226.v1>
11. Thuy BTP, My TTA, Hai NTT, Hieu LT, Hoa TT, Loan TPH, Nhung NTA (2020) Investigation into SARS-CoV-2 resistance of compounds in garlic essential oil. *ACS Omega* 5(14):8312–8320. <https://doi.org/10.1021/acsomega.0c00772>
12. Zumla A, Chan JF, Azhar EI, Hui DS, Yuen KY (2016) Coronaviruses—drug discovery and therapeutic options. *Nat Rev Drug Discov* 15(5):327–347. <https://doi.org/10.1038/nrd.2015.37>
13. Elfiky AA (2021) SARS-CoV-2 RNA dependent RNA polymerase (RdRp) targeting: an in silico perspective. *J Biomol Struct Dyn* 39(9):3204–3212. <https://doi.org/10.1080/07391102.2020.1761882>
14. Furuta Y, Gowen BB, Takahashi K, Shiraki K, Smee DF, Barnard DL (2013) Favipiravir (T-705), a novel viral RNA polymerase inhibitor. *Antiviral Res* 100(2):446–454. <https://doi.org/10.1016/j.antiviral.2013.09.015>
15. Tözser J (2010) Comparative studies on retroviral proteases: substrate specificity. *Viruses* 2(1):147–165. <https://doi.org/10.3390/v2010147>
16. Li G, De Clercq E (2020) Therapeutic options for the 2019 novel coronavirus (2019-nCoV). *Nat Rev Drug Discov* 19(3):149–150. <https://doi.org/10.1038/d41573-020-00016-0>
17. Zhang T, Wu Q, Zhang Z (2020) Probable pangolin origin of SARS-CoV-2 associated with the COVID-19 outbreak. *Curr Biol CB* 30(7):1346–1351.e2. <https://doi.org/10.1016/j.cub.2020.03.022>
18. Alotheid H, Aldughaim MSK, El Bakkouri K, AIMashhadi S, Al-Qahtani AA (2020) Similarities between the effect of SARS-CoV-2 and HCV on the cellular level, and the possible role of ion channels in COVID19 progression: a review of potential targets for diagnosis and treatment. *Channels (Austin)* 14(1):403–412. <https://doi.org/10.1080/19336950.2020.1837439>
19. Sliwoski G, Kothiwale S, Meiler J, Lowe EW Jr (2014) Computational methods in drug discovery. *Pharmacol Rev* 66(1):334–395. <https://doi.org/10.1124/pr.112.007336>
20. Hajduk PJ, Huth JR, Tse C (2005) Predicting protein druggability. *Drug Discov Today* 10(23–24):1675–1682. [https://doi.org/10.1016/S1359-6446\(05\)03624-X](https://doi.org/10.1016/S1359-6446(05)03624-X)
21. Laskowski RA, MacArthur MW, Moss DS, Thornton JM (1993) PROCHECK: a program to check the stereochemical quality of protein structures. *J Appl Cryst* 26:283–291
22. Dallakyan S, Olson AJ (2015) Small-molecule library screening by docking with PyRx. *Methods Mol Biol (Clifton, NJ)* 1263:243–250. https://doi.org/10.1007/978-1-4939-2269-7_19
23. Trott O, Olson AJ (2010) AutoDock Vina: improving the speed and accuracy of docking with a new scoring function, efficient optimization, and multithreading. *J Comput Chem* 31(2):455–461. <https://doi.org/10.1002/jcc.21334>
24. Kalé L, Skeel R, Bhandarkar M, Brunner R, Gursoy A, Krawetz N, Schulten K (1999) NAMD2: greater scalability for parallel molecular dynamics. *J Comput Phys* 151(1):283–312. <https://doi.org/10.1006/jcph.1999.6201>
25. Bowers KJ, Chow DE, Xu H, Dror RO, Eastwood MP, Gregersen BA, Shaw DE (2006) Scalable algorithms for molecular dynamics simulations on commodity clusters. In: *ACM/IEEE SC 2006 Conference (SC'06)*. Presented at the SC 2006 Proceedings Supercomputing 2006, Tampa, FL. <https://doi.org/10.1109/sc.2006.54>
26. Ferreira LG, Dos Santos RN, Oliva G, Andricopulo AD (2015) Molecular docking and structure-based drug design strategies. *Mol (Basel Switz)* 20(7):13384–13421. <https://doi.org/10.3390/molecules200713384>
27. Hildebrand PW, Rose AS, Tiemann JKS (2019) Bringing molecular dynamics simulation data into view. *Trends Biochem Sci* 44(11):902–913. <https://doi.org/10.1016/j.tibs.2019.06.004>
28. Rasheed MA, Iqbal MN, Saddick S, Ali I, Khan FS, Kanwal S, Awais M (2021) Identification of lead compounds against scm (fms10) in *Enterococcus faecium* using computer aided drug designing. *Life (Basel Switz)* 11(2):77. <https://doi.org/10.3390/life11020077>
29. Shivakumar D, Williams J, Wu Y, Damm W, Shelley J, Sherman W (2010) Prediction of absolute solvation free energies using molecular dynamics free energy perturbation and the OPLS force field. *J Chem Theory Comput* 6(5):1509–1519. <https://doi.org/10.1021/ct900587b>
30. Tripathi MK, Ahmad S, Tyagi R, Dahiya V, Yadav MK (2022) Fundamentals of molecular modeling in drug design. In: *Computer aided drug design (CADD): from ligand-based methods to structure-based approaches*, pp 125–155. <https://doi.org/10.1016/b978-0-323-90608-1.00001-0>
31. Alturki NA, Mashraqi MM, Alzamami A, Alghamdi YS, Alharthi AA, Asiri SA, Alshamrani S (2022) In-silico screening and molecular dynamics simulation of Drug Bank experimental compounds against SARS-CoV-2. *Mol (Basel Switz)* 27(14):4391. <https://doi.org/10.3390/molecules27144391>
32. Ahmad S, Bano N, Qazi S, Yadav MK, Ahmad N, Raza K (2022) Multitargeted molecular dynamic understanding of Butoxypheser against SARS-CoV-2: an in silico study. *Nat Prod Commun* 17(7):1934578X2211154. <https://doi.org/10.1177/1934578x221115499>
33. Barh D, Tiwari S, Rodrigues Gomes LG, Ramalho Pinto CH, Andrade BS, Ahmad S, Tambuwala MM (2023) SARS-CoV-2 variants show a gradual declining pathogenicity and pro-inflammatory cytokine stimulation, an increasing antigenic and anti-inflammatory cytokine induction, and rising structural protein instability: a minimal number genome-based approach. *Inflammation* 46(1):297–312. <https://doi.org/10.1007/s10753-022-01734-w>
34. Tarique M, Ahmad S, Malik A, Ahmad I, Saeed M, Almatroudi A, Al-Saleh Y (2021) Novel severe acute respiratory syndrome Coronavirus 2 (SARS-CoV2) and other coronaviruses: a genome-wide comparative annotation and analysis. *Mol Cell Biochem* 476(5):2203–2217. <https://doi.org/10.1007/s11010-020-04027-8>
35. Jin Z, Du X, Xu Y, Deng Y, Liu M, Zhao Y, Yang H (2020) Structure of Mpro from SARS-CoV-2 and discovery of its inhibitors. *Nature* 582(7811):289–293. <https://doi.org/10.1038/s41586-020-2223-y>
36. Falade VA, Adelusi TI, Adedotun IO, Abdul-Hammed M, Lawal TA, Agboluaje SA (2021) In silico investigation of saponins and tannins as potential inhibitors of SARS-CoV-2 main protease (Mpro). In *Silico Pharmacol* 9(1):9. <https://doi.org/10.1007/s40203-020-00071-w>

Publisher's Note

Springer Nature remains neutral with regard to jurisdictional claims in published maps and institutional affiliations.